Applied Physics B (2020) 126:141
https://doi.org/10.1007/s00340-020-07445-0

Applied Physics B
Lasers and Optics

CO_2 laser system design for efficient boron isotope separation by the method of selective laser-assisted retardation of condensation

K. A. Lyakhov[1] · **A. N. Pechen**[1,2]

Received: 27 August 2019 / Accepted: 20 April 2020

Abstract
A cheap and efficient production of boron isotopes is important for providing further progress in nuclear engineering, semiconductor industry, and nuclear medicine. Motivated by this problem, we consider the CO_2 laser system designed to separate boron isotopes by the method of laser-assisted retardation of condensation. Values of the basic parameters for this system, such as an acceptable variation range of the laser operating pressure, mode locking laser system design, and estimation of an acceptable interval for the variation of laser intensity for various positions of the photo-absorption lines of BCl_3, corresponding to ambiguity of available experimental data, are found. To calculate them, a new formalism, which takes into account spectral shape of photo-absorption cross section and laser pulse emission spectrum, is developed. Conclusion that the three-line excitation is the most efficient one has been derived.

1 Introduction

Boron isotopes have various application in nuclear, semiconductor and medical industries. For instance, a small amount of boric acid used as a neutron poison injected in the coolant in commonly used pressurized water reactors reduces corrosion and wear of the reactor core thereby allowing for a longer fuel cycle and smaller maintenance cost. Small amount of boron enriched BCl_3 or BF_3 used for silicon doping allows to make doped silica matrix more isotopically uniform thereby increasing its heat conductivity, which becomes crucial with advancing miniaturization of electronic devices [1]. Boron nanowires [2] and borophene (2D boron) [3] were proposed for using in the emerging field of flexible electronics because their electrical properties are robust under strain. Enriched boron can improve performance of a flexible microelectronic device due to increased heat conductivity. Using isotopically enriched boron can significantly enhance solar panel efficiency due to its temperature dependence [4, 5]. Small amount of intravenously administrated boron to tumor delivering agent allows to make boron neutron capture cancer therapy more efficient [6–8].

Motivated by the dependence of excitation rate of molecules on the laser pulse shape, [9, 10], the goal of this paper is to design a laser system, which can provide desired spectral characteristics of the laser pulse to separate boron isotopes efficiently within the method of selective laser-assisted retardation of condensation (SILARC) [11, 12]. Target isotopes can be selectively excited by the photons of appropriate frequency. In contrast to such popular laser-assisted methods such as molecule obliteration laser isotope separation (MOLIS) and atomic vapor laser isotope separation (AVLIS), large laser fluence is not required and even should be avoided in the SILARC method due to destructive resonant interaction of strong electric fields with target molecules. Ideally, laser intensity should be just high enough for molecular excitation, and, therefore, able to guide molecular dynamics in the desired direction [9]. This method is potentially more energy efficient, because of a higher excitation rate due to typically two orders of magnitude larger cross-section, which corresponds to linear photo-absorption, than for non-linear absorption, which corresponds to multi-photon dissociation [13].

In the SILARC method, target gas molecules are mixed with carrier gas at rather small molar fraction to prevent nearly resonant vibration–vibrational excitation loss, leading

✉ K. A. Lyakhov
lyakhov2000@yahoo.com

[1] Department of Mathematical Methods for Quantum Technologies, Steklov Mathematical Institute of Russian Academy of Sciences, Gubkina str. 8, Moscow 119991, Russia

[2] National University of Science and Technology "MISIS", Leninskii Av. 4, Moscow 119049, Russia

Published online: 30 July 2020

to selectively excited isotopes scrambling effect. In this method, isotope harvesting is based on the fact that lighter species diffuse to the gas flow periphery faster than heavier species. Hence, heavy and light species are fully separated by the end of the gas flow, corresponding to skimmer inlet position, and further separately pumped out towards related cold traps. The mass difference between light (monomers) and heavy (dimers) species can be controlled by applying laser beam radiation to the overcooled gas flow. Selective action of the laser beam relies upon resonant energy absorption of laser photons by target isotopologues,[1] preventing their condensation, which would occur otherwise. In dilute overcooled gas flow, collisional broadening is dominant and photo-absorption spectra are very narrow.

In SILARC method, the choice of target gas molecules and carrier gas plays an essential role. We consider BCl_3 as a target gas molecule due to excitability of its spectrum by CO_2 laser and high enough vapor pressure at room temperature. However, caution must be exercised to keep dry vacuum conditions, because BCl_3 is not hydrolysis resistant. It should be mentioned that other laser systems, which can emit in infrared region, such as optical fiber and diode lasers on heterostructures, that are used as a pump for the optical parametric oscillator, quantum cascade (QC), and free electron lasers are even more attractive to use, because they can provide higher selectivity due to their continuous tunability, which is important, because the absorption bandwidth of BCl_3 molecules in rarefied overcooled gas flow is very narrow. On the other hand, these systems are much more expensive than mode locked CO_2 laser, considered in this paper, and power output is much more limited: $0.1 \div 10$ mW and ≤ 1 W for diode and QC lasers, respectively. Moreover, its efficiency is significantly higher, which is more important for industrial applications.

Argon is chosen as a carrier gas because of its excellent aerodynamic properties. At room temperature, fundamental vibrational modes $\nu_3 \equiv^{11} \nu_{3;n}$ of isotopologues $^{11}B^{35}Cl_n^{37}Cl_{3-n} \equiv (35)^n(37)^{3-n}; n = 1, 2, 3$ can be readily excited by the following CO_2 laser lines: 10P(4)-10P(28). For laser intensities lower than saturation limit, 10P(8)–10P(16) lines are better absorbed [14], while at large laser intensities, when multi-photon processes become more important, photo-absorption maximums are red-shifted so that using of 10P(24)–10P(28) lines is more appropriate, [15–17]. By increasing the operating pressure of the laser medium, frequency mismatches can be compensated due to spectral line broadening. If gas flow pressure is too high, then, due to collision rate, the rate of excitation loss equals to, or even lower than, the rate of excitation gain. Moreover, if gas flow temperature is too high, then hot rotational bands are strongly populated. Hence, to decrease these effect, irradiated gas flow should be sufficiently dilute and cold.

To enhance boron isotopes recovery, multi-line excitation of BCl_3, having four photo-absorption peaks, related to different combinations of boron-11 with chlorine isotopes, can be used. A new laser system, employing mode-locking technique, to implement this is proposed. Use of multi-line infrared excitations for laser-assisted isotope separation has already been considered in some other works, e.g., for separation of tritium by selective multi-photon excitation of rotational lines, which leads to a subsequent dissociation of target gas molecules [18].

To use laser photons more efficiently, we assume that the gas flow is irradiated cross-wise in a multi-pass cavity, so that the laser beam oscillates between two mirrors installed on the opposite walls of irradiation chamber. The research on carbon and boron isotope separation in a multi-pass cavity was performed also, for example, in Refs. [19, 20].

This paper is organized as follows. In Sect. 1, the operational principles of the experimental setup for boron isotopes separation are described. In Sect. 2, linear photo-absorption cross sections for different BCl_3 isotopologues are derived from the available experimental data. In Sect. 3, gas flow irradiation conditions and constraints on the related laser system are discussed. In Sect. 4, the physical parametrization of the laser pulse spectrum and its evolution in the multi-pass resonant cavity are given. In Sect. 5, a new formula for the multi-line excitation rate is derived and used to derive the conditions for laser intensity variation range, which corresponds to applicability of the SILARC method.

2 Boron isotope separation setup operational principles

The operational scheme of the setup is presented in Fig. 1. Proposed design is similar to the one from Ref. [20], unless whole gas flow is irradiated there and single-line excitation is applied. At the beginning of operation, the mixing tank is occupied only by the carrier gas (Ar) at room temperature T_0, while target gas molecules (BCl_3), having initially natural relative isotope abundance, are stored in the feed chamber. Then BCl_3 is injected into the mixing tank. BCl_3 is seeded at a very low molar fraction $\mu \sim 0.02$ into argon to minimize nearly resonant vibration–vibration (VV) excitation loss caused by collisions among BCl_3 molecules. Moreover, gas flow itself should be diluted high enough to minimize vibration–translational (VT) relaxation. Gas flow pressure p_{flow} and temperature T_{flow} are assumed maintained close to the following values $p_{\text{flow}} = 10$ mTorr and $T_{\text{flow}} = 50$ K.

Gas flow expands continuously from the mixing tank into irradiation cell, where it is irradiated cross-wise by the laser

[1] Isotopologue of a chemical species has at least one atom with a different number of neutrons.

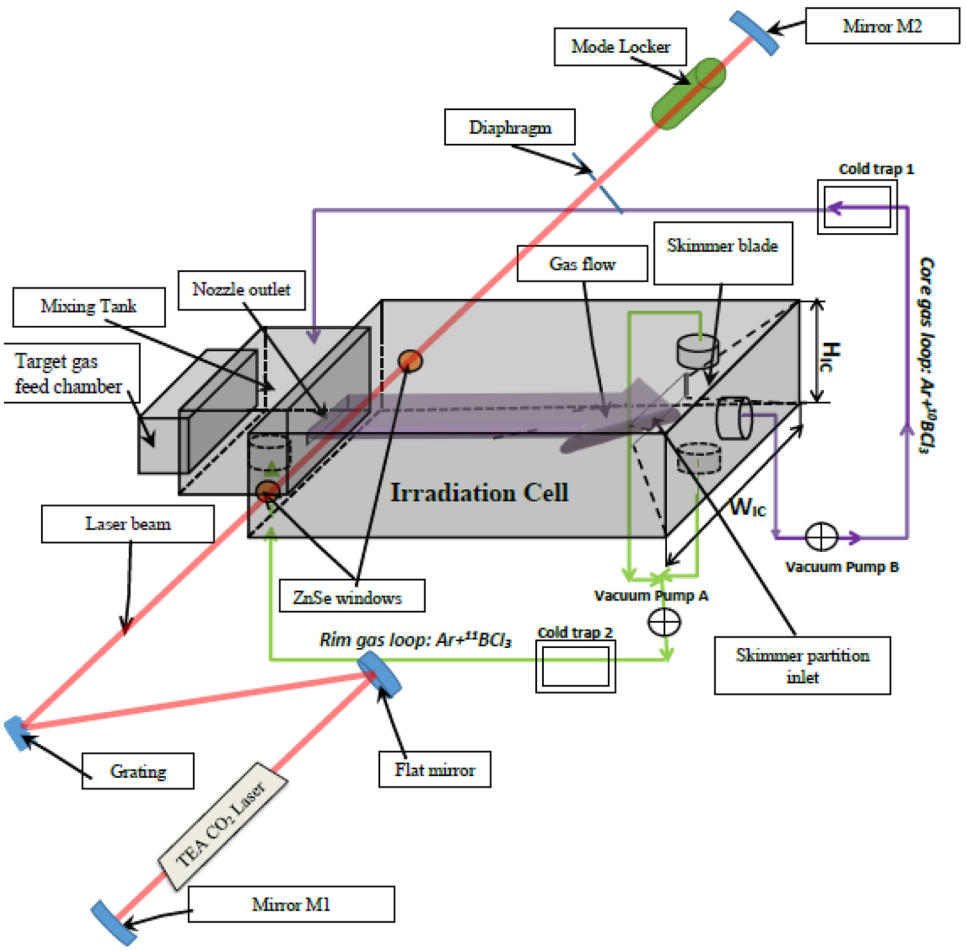

Fig. 1 The principal scheme of the boron isotope separation setup, based on the method of laser-assisted retardation of condensation (edges, links and details that are invisible from the frontal surface are displayed by dashed lines). The laser beam passes through the semi-transparent window and cross-wise impinges the gas flow. To increase the excitation rate, laser beam oscillates back and forth within the resonant multi-pass cavity. Core gas is boron-10 enriched by selective laser evaporation of $^{11}BCl_3$ isotopologues. The gas circulates from the mixing tank and back to compensate pressure loss and to achieve higher recovery of target isotopes. Radius curvature of the mirrors M1 and M2 is assumed to be 2500 mm

beam. To generate short multi-line pulses, mode-locking by one-grating configuration can be implemented as proposed in Ref. [21]. In this case, the laser beam is confined between one flat and two concave mirrors and grating, as shown in Fig. 1.

To irradiate the largest volume of the gas flow maintaining the optimal static pressure and temperature fields, a uniform velocity profile should be provided by specially designed slit nozzle profile.

Skimmer blade divides the gas flow into target isotope (boron-11) enriched (rim) and desired isotope (boron-10) enriched (core) fractions. Each fraction, having laser controlled target isotopologue populations, is pumped out by respective vacuum pump, which has appropriately chosen pumping down rate. Before BCl_3 is redirecting back into the mixing tank, it is partially captured by the respective cold traps, assigned for target isotope enriched and depleted gas flow fractions.

3 Evaluation of BCl_3 photo-absorption cross section

Linear differential photo-absorption cross section σ_A for each line, corresponding to different chlorine isotopologues of BCl_3, is related to infrared intensity I_{IR}, which can be introduced through Napierian absorbance[2] $A_e(\tilde{\lambda})$, which is Napierian, or natural, logarithm of the ratio of intensities of incident I_0 and transmitted light $I(\tilde{\lambda})$, as

$$I_{IR} = \frac{1}{n_i d}\int A_e(\tilde{\lambda})\mathrm{d}\tilde{\lambda} = \int \sigma_A(\tilde{\lambda})\mathrm{d}\tilde{\lambda},\ \sigma_A(\tilde{\lambda}) = \sum_{k=1}^{4}\sigma_k,\quad \sigma_k \equiv \sigma_A(\tilde{\lambda},\tilde{\lambda}_k), \tag{1}$$

where $n_i = \mu x_i n_{gas}$ is concentration of $^{11}BCl_3$, d-optical path length, $\tilde{\lambda}_k$ is the wavenumber for excitation of the ν_3 fundamental vibrational mode, related to kth isotopologue

[2] More details can be found in Ref. [22].

Table 1 Wavenumbers of CO_2 laser emission and BCl_3 absorption line maximums corresponding to the choice $\tilde{\lambda}_1 = \tilde{\lambda}_{1,\max}$

CO_2 laser emission line specification$\Rightarrow \tilde{\lambda}_{k;\mathrm{las}}$, cm^{-1}	BCl_3 absorption line specification$\Rightarrow \tilde{\lambda}_k$, cm^{-1}
$10P(4) \Rightarrow 957.8$	$(35)^3 + (35)^2(37) \Rightarrow 957.67$
$10P(6) \Rightarrow 956.185$	$(35)^2(37) \Rightarrow 956.256$
$10P(8) \Rightarrow 954.545$	$(37)^2(35) \Rightarrow 955.07 (37)^3 + (37)^2(35) \Rightarrow 953.76$

$(k = 1, 2, 3, 4)$. According to experimental data from Ref. [23], $I_{\mathrm{IR}} = 231.3\,\mathrm{km/mol}$.

Absorption line full width at half of maximum (FWHM), caused by collisional broadening solely, is given by

$$\Delta\tilde{\lambda}_{\mathrm{c}} = 2\gamma = \frac{10^{-2}\Delta\nu_c}{c} = 0.84 \times 10^{-4}\,\mathrm{cm}^{-1}, \tag{2}$$

$$\Delta\nu_{\mathrm{c}} = 2n_{\mathrm{gas}}\left(\sigma_{\mathrm{QG}}(1-\mu)\sqrt{\frac{8RT_{\mathrm{flow}}}{\pi M_{\mathrm{QG}}}} + \sigma_{\mathrm{QQ}}\mu\sqrt{\frac{8RT_{\mathrm{flow}}}{\pi M_{\mathrm{QQ}}}}\right). \tag{3}$$

Here $n_{\mathrm{gas}} = \frac{p_{\mathrm{flow}}}{k_{\mathrm{B}}T_{\mathrm{flow}}}$, $M_{\mathrm{QQ}} = 58.6\,\mathrm{g/mol}$ and $M_{\mathrm{QG}} = 29.8\,\mathrm{g/mol}$ are the reduced molar masses for collisions of target (Q) and carrier (G) gas molecules, $\sigma_{\mathrm{QQ}} = 340\,\text{Å}^2$ and $\sigma_{\mathrm{QG}} = 233.3\,\text{Å}^2$ are respective cross sections. Absorption line full width at half of maximum (FWHM), caused by Doppler broadening solely, is given by

$$\Delta\tilde{\lambda}_{D;k} = \sigma_{0;k}\sqrt{8\ln 2} = \frac{10^{-2}\Delta\nu_{D;k}}{c} = 3.66 \times 10^{-4}\,\mathrm{cm}^{-1},$$
$$\Delta\nu_{D;k} = \tilde{\lambda}_k\sqrt{\frac{8\ln 2 R_B T_{\mathrm{flow}}}{M_Q^k}}. \tag{4}$$

Therefore, both effects are comparable at considered gas flow pressure, temperature, and photo-absorption cross section can be estimated by Voigt distribution,

$$\sigma_k(\tilde{\lambda}) = \sigma_{k;\max}\frac{\gamma}{\pi\sqrt{2\pi}\sigma_{0;k}}\int_{-\infty}^{\infty}\frac{\exp\left\{\frac{-\tilde{\lambda}'^2}{2\sigma_{0;k}^2}\right\}}{(\tilde{\lambda}-\tilde{\lambda}_k-\tilde{\lambda}')^2+\gamma^2}\mathrm{d}\tilde{\lambda}'. \tag{5}$$

Absorption line full width at half of maximum can be approximated as

$$\Delta\tilde{\lambda}_{V;k} = \frac{10^{-2}}{c}\left(0.535 + \sqrt{0.2166\Delta\nu_c^2 + \Delta\nu_{D;k}^2}\right) = 4.13 \times 10^{-4}\,\mathrm{cm}^{-1}. \tag{6}$$

As follows from Eq. (1), the maximum of photo-absorption cross section for kth isotopologue is given by

$$\sigma_{k;\max} = I_{\mathrm{IR}}p_k. \tag{7}$$

The $(35)^n(37)^{3-n}$ isotopologues belong to one of the two symmetry groups, D_{3h} or C_{2v}, depending on whether the masses of chlorine isotopes are equal or not. Thus, the photo-absorption lines corresponding to $\tilde{\lambda}_1$ and $\tilde{\lambda}_4$ are contributed by both $(35)^2(37)$ and $(35)(37)^2$, because of double-line splitting. Therefore, the respective absorption peak intensities are proportional to the following probabilities[3]

$$p_1 = P((35)^3) + 1.5P((35)^2(37)) = 0.64 \tag{8}$$

$$p_4 = P((37)^3) + 1.5P((35)(37)^2) = 0.08, \tag{9}$$

while intermediate peaks at $\tilde{\lambda}_2$ and $\tilde{\lambda}_3$ are just proportional to

$$p_2 = 1.5P((35)^2(37)) = 0.21 \tag{10}$$

and

$$p_3 = 1.5P((35)(37)^2) = 0.06, \tag{11}$$

respectively. Here, probabilities to find ^{35}Cl and ^{37}Cl isotopes in natural blend are $P(35) = 0.76$ and $P(37) = 0.24$, respectively. Probability to find specific blend of chlorine isotopes is denoted by $P(35^n37^{3-n})$, $n = 1 \cdots 3$.

This gives the following maximums of photo-absorption cross sections for various combinations of chlorine isotopes:

$$\{\sigma_{1;\max}, \sigma_{2;\max}, \sigma_{3;\max}, \sigma_{4;\max}\} = \{520;169;54.12;65.73\}\,\text{Å}^2. \tag{12}$$

4 Experimental constraints on the laser system design

Precise experimental identification of the photo-absorption line center position $\tilde{\lambda}_1$ of the gaseous state $^{11}BCl_3$ is ambiguous so far. It ranges from $\tilde{\lambda}_{1,\max} = 957.67\,\mathrm{cm}^{-1}$, according to Ref. [15], to $\tilde{\lambda}_{1,\min} = 954.2\,\mathrm{cm}^{-1}$, according to Ref. [23]. We will use the both extremes[4] to estimate the appropriate laser intensity range for the designed CO_2 laser system. Mutual dispositions of the laser emission and BCl_3 photo-absorption line peaks, corresponding to the both extremes, are shown in Tables 1 and 2. The distances between neighbor peaks

[3] Probability to find combination of $^{35}Cl_n$ and $^{37}Cl_{3-n}$ is denoted by $P((35)^n(37)^{3-n})$.

[4] IR-shifted value $944.194\,\mathrm{cm}^{-1}$, which was measured in Ref. [17], can be explained by a multi-photon absorption at high vibrational temperature.

Table 2 Wavenumbers of CO_2 laser emission and BCl_3 absorption line maximums corresponding to the choice $\tilde{\lambda}_1 = \tilde{\lambda}_{1,\min}$

CO_2 laser emission line specification⇒ $\tilde{\lambda}_{k;\text{las}}$, cm^{-1}	BCl_3 absorption line specification⇒ $\tilde{\lambda}_k$, cm^{-1}
$10P(8) \Rightarrow 954.545$	$(35)^3 + (35)^2(37) \Rightarrow 954.2$
$10P(10) \Rightarrow 952.881$	$(35)^2(37) \Rightarrow 952.79$
$10P(12) \Rightarrow 951.1922$	$(37)^2(35) \Rightarrow 951.597$

corresponding to different combinations of chlorine isotopes are taken from the experimental data for BCl_3 frozen in argon matrix [24]:

$$\begin{aligned}\Delta\tilde{\lambda}_{12} &= 1.41\,\text{cm}^{-1};\\ \Delta\tilde{\lambda}_{23} &= 1.189\,\text{cm}^{-1};\\ \Delta\tilde{\lambda}_{34} &= 1.301\,\text{cm}^{-1}.\end{aligned} \tag{13}$$

If $\tilde{\lambda}_1 = \tilde{\lambda}_{1,\max}$ is assumed, then according to Table 1, to overlap[5] with the related photo-absorption spectrum, the minimal values of FWHM of 10P(4)–10P(10) laser lines should be

$$\Delta\tilde{\lambda}_{k,\text{FWHM}} = \{0.26; 0.142; 1.05; 1.57\}\,\text{cm}^{-1}. \tag{14}$$

As can be seen, lines 10P(4)–10P(8) are the nearest to the related photo-absorption lines (line 10P(10) would require too high laser medium operational pressure). However, only single-line excitation is feasible, because intensity only of the line 10P(8) is perceptible in the given interval of wavelengths for modern CO_2 lasers [25], unless specific combination of isotopically pure carbon and oxygen is used [21]. Depending on the pressure in the laser medium, it can be used either for one ($(37)^2(35)$, laser line FWHM should be at least $\Delta\tilde{\lambda}^{\max}_{\text{FWHM}} = 1.05\,\text{cm}^{-1}$) or two ($(37)^2(35) + (37)^3$ and $(37)^3$, laser line FWHM should be at least $\Delta\tilde{\lambda}^{\max}_{\text{FWHM}} = 1.31\,\text{cm}^{-1}$) photo-absorption lines excitation.

FWHM of roto-vibrational transition lines of CO_2 laser can be estimated by the following formula, which takes into account dependence on temperature T_{las} and pressure P_{las} (in hPa) in the laser medium along with angular momentum J, corresponding to the given rotational line:

$$\begin{aligned}&\Delta\nu_{\text{FWHM}}\,[\text{MHz}]\\ &= 2P_{\text{las}}\,[\text{hPa}](\Psi_{\text{CO}_2}b_{\text{CO}_2} + \Psi_{N_2}b_{\text{N}_2} + \Psi_{\text{He}}b_{\text{He}})\left(\frac{300}{T_{\text{las}}}\right)^{\bar{n}},\end{aligned} \tag{15}$$

where $\bar{n} = 0.58$, and laser medium composition $\Psi_{\text{CO}_2} : \Psi_{\text{N}_2} : \Psi_{\text{He}} = 1 : 1 : 3$ were assumed. Here, $\Psi_{\text{He;N}_2;\text{CO}_2}$ are the molar fractions of the constituent gases, and

$$\begin{aligned}b_{\text{CO}_2} &= 3.4 - |m| \cdot 0.0272,\\ b_{\text{He}} &= 1.77 - |m| \cdot 0.00083,\\ b_{\text{N}_2} &= 2.35 - |m| \cdot 0.0127,\end{aligned}$$

where $m = -J$ for P-branch and $m = J + 1$ for R-branch. However, formula (15) is not applicable, if either $T_{\text{las}} > 470\,\text{K}$, when level 100 is overpopulated (population inversion cannot be maintained), or $P_{\text{las}} > 12 \div 15\,\text{bar}$, when plasma discharge gets unstable.[6] For our estimations we assume, that cooling system can stabilize laser medium temperature at $T_{\text{las}} = 350\,\text{K}$. Then the operating pressure, which corresponds to two photo-absorption lines excitation, should be not higher than $P_{\text{las}} = 13\,\text{bars}$. According to Eq. 15, one has for one-line excitation $P_{\text{las}} = 8.16\,\text{bar}$, and for two-line excitation $P_{\text{las}} = 12.75\,\text{bars}$.

If $\tilde{\lambda}_1 = \tilde{\lambda}_{1,\min}$ is assumed, then according to Table 2, linewidths of the lines 10P(8)–10P(14) should be

$$\Delta\tilde{\lambda}_{k,\text{FWHM}} = \{0.69; 0.19; 0.81; 1.632\}\,\text{cm}^{-1}. \tag{16}$$

Hence, lines 10P(8)–10P(12) can be used for simultaneous excitation of chlorine isotopologues, provided laser operating pressure is $P_{\text{las}} = 5.7\,\text{bars}$, which corresponds to $\Delta\tilde{\lambda}^{\max}_{\text{FWHM}} = 0.81\,\text{cm}^{-1}$.

Mode-locking can be used for a multi-line laser pulse generation [26, 29]. Mode-locked laser system pulse width τ_{p} can be computed as

$$\tau_{\text{p}} \approx 0.45\left(\frac{g}{M}\right)^{\frac{1}{4}}\frac{1}{\sqrt{f\Delta\nu_{\text{FWHM}}}}, \tag{17}$$

where M is the modulation amplitude, $f = c/2L$ is its frequency, L is the resonator length, $g = 2aL$ is the saturated round-trip excess gain, a is the excess gain per unit length. We assume $g = M = 1$ and $L = 3\,\text{m}$ [30]. This corresponds to the laser pulse width $\tau_{\text{p}} = 9.7\,\text{ps}$ for excitation of $(37)^2(35)$ or $\tau_{\text{p}} = 6.2\,\text{ps}$ for excitation $(37)^2(35)$ and $(37)^3 + (37)^2(35)$ both, corresponding to the choice $\tilde{\lambda}_{1,\max}$ (one-line excitation), or $\tau_{\text{p}} = 14.11\,\text{ps}$ corresponding to the choice $\tilde{\lambda}_{1,\min}$ (three-line excitation).

[5] Henceforth, overlapping at least at half of maximum of laser intensity is assumed.

[6] Design of the cavity containing a 10-atm TE discharge CO_2 laser amplifier module was reported in Refs. [26, 27] and 12-atm in Ref. [28].

5 Relation of multi-frequency CO_2 laser pulse shape with BCl_3 photo-absorption cross section

Time evolution of the laser intensity $I(t)$ inside the cavity can be evaluated by

$$I(t) = \frac{c\epsilon_0 n|E(t)|^2}{2}. \tag{18}$$

Here n is irradiation cell (IC) ambient gas refractivity index, and $E(t)$ is the electric field in vacuum.

Since the laser beam is confined between two parallel mirrors, which form a multi-pass resonant optical cavity, the electric field at some fixed time is a superposition of the electric fields from the previously emitted laser pulses over the total time interval elapsed t:

$$E(t) = \sum_{j=0}^{N_p(t)} E^{(j)}(t). \tag{19}$$

Here $N_p(t)$ is the number of laser pulses emitted. Multi-line laser pulse electric field strength with $N_l = \{1;3\,\text{or}\,4\}$ laser emission lines can be decomposed as

$$E^{(j)}(t) = \sum_{k=1}^{N_l} E^{(jk)}(t). \tag{20}$$

The number of the laser pulses $N_p(t)$ can be calculated as the upper bound of the ratio t/T_p, where the length of the laser pulse train is $T_p = 1/f = 20$ ns. The interaction time of the laser pulse of radius R_L 1.1 mm with the gas flow is given by

$$\tau_{int} = \frac{2R_L}{\langle v\rangle} = 4\,\mu\text{s}. \tag{21}$$

Here average velocity of a gas molecule is

$$\langle v\rangle = \sqrt{\frac{2\gamma RT_{flow}}{M_G(\gamma-1)}\left(\frac{T_0}{T_{flow}}-1\right)}, \tag{22}$$

where $\gamma = 1.617$ is the specific heat ratio of $BCl_3 + Ar$ mixture and M_G is argon molar mass. Thus, the number of laser pulses emitted over τ_{int} is $N_p(\tau_{int}) = 606$.

Following Ref. [31], we assume Gaussian envelope for mode intensities. Thus, total electric field strength of mode-locked laser pulses is

$$E^{(jk)}(x,t) = E_0^{(k)}\boldsymbol{\Phi}^{(jk)}(x,t), \tag{23}$$

where $E_0^{(k)}$ is the electric field amplitude and

$$\boldsymbol{\Phi}^{(jk)}(x,t) = \frac{1}{2\pi}\int_{-\infty}^{\infty} d\omega Q_{las}(\omega,x,t)\mathcal{F}_k(\omega)e^{i\omega t_{jk}}, \tag{24}$$

$$\mathcal{F}_k(\omega) = \frac{\sqrt{8\pi\ln 4}}{\Delta\omega_p}\exp\left\{-2\ln 4\frac{(\omega-\omega_{k;las})^2}{\Delta\omega_p^2}\right\}, \tag{25}$$

$$t_{jk} = t - jT_p - \tau_r^{(jk)}. \tag{26}$$

Here, imaginary unit is denoted by i, $\omega_{k;las} = 2\pi\nu k;las = 2\pi c\tilde{\lambda}_{k;las}$, and $\Delta\omega_p$ is the laser pulse bandwidth. Inverse population build-up times $\tau_r^{(jk)}$ correspond to different transition lines $k = 1,\ldots,N_l$ and fluctuate from pulse to pulse, according to some random process $\phi_{jk}(x,t)$. As a result, stability of the laser pulse power can be rather poor. To circumvent this problem, optical path length can be modulated by retro-mirror position(one of the three mirrors shown in Fig. 1), which is controlled by periodic voltage, applied to piezoelectric transducer (PZT). Alternatively, retro-mirror position can be automatically controlled by a phase-shift sensitive detector, which can be used to run generator, activating PZT.

Since, according to the experimental data from Ref. [32], the product of an AM mode-locked laser pulse length and bandwidth is smaller than the value for Gaussian pulses, estimated in Refs. [30, 31], $\Delta\nu_p\tau_p = 2\ln 2/\pi$, in 1.423 times, laser pulse bandwidth can be estimated as $\Delta\omega_p \approx 1.95/\tau_p$.

As a next step, we take an average of Eq. (18) over the length of intersection between the laser beam and the gas flow:

$$I(t) = \frac{c\epsilon_0 n}{2}\left\{\sum_{i_1=1}^{N_l}\sum_{i_2=1}^{N_l} E_0^{(i_1)}E_0^{(i_2)}\langle\aleph^{(i_1)}\tilde{\aleph}^{(i_2)}\rangle_x\right\}. \tag{27}$$

Here

$$\aleph^{(k)}(x,t) = \sum_{j=0}^{N_p(t)}\boldsymbol{\Phi}^{(jk)}(x,t), \quad \tilde{\aleph}^{(k)}(x,t) = \sum_{j=0}^{N_p(t)}\tilde{\boldsymbol{\Phi}}^{(jk)}(x,t), \tag{28}$$

$$\tilde{\boldsymbol{\Phi}}^{(jk)}(x,t) = \frac{1}{2\pi}\int_{-\infty}^{\infty} d\omega\overline{Q}_{las}(\omega,x,t)\mathcal{F}_k(\omega)e^{i(\omega t_{jk}+\phi_{jk}(x,t))}, \tag{29}$$

where $\bar{f}$ means complex conjugate and averaging is carried out as

$$\langle f\rangle_x = \frac{\cos\alpha}{W_f}\int_{\delta}^{\delta+W_f} f(x)dx. \tag{30}$$

Here α is the angle between laser pulse and the direction of the gas flow, $W_f = 5$ cm is the width of gas flow, and

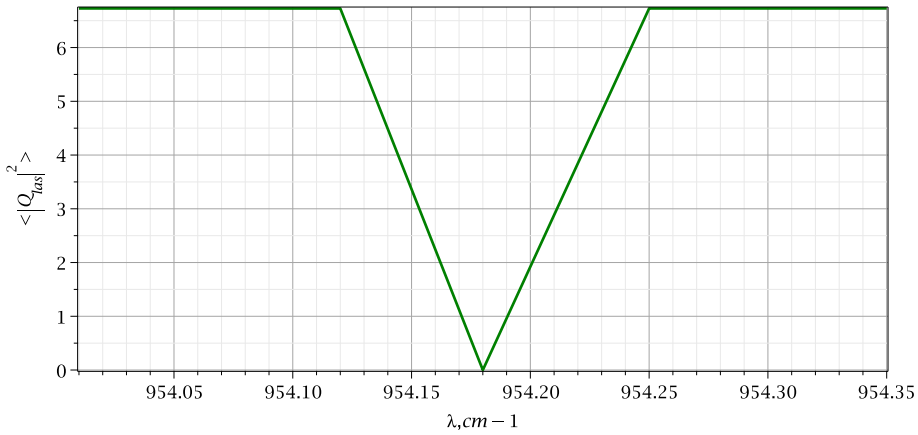

Fig. 2 Spectrum of amplification factor squared $\langle |Q_{\rm las}|^2 \rangle_x$, calculated after the first laser pulse, and averaged over transverse coordinate, according to Eq. (30). Laser pulse spectrum corresponds to three-line excitation ($\tilde{\lambda}_{1,\min}$)

$\delta = 4.81$ cm is the distance between the cold core surface of the gas flow and irradiation cell wall.

By taking into account that

$$\mathfrak{Z}(\omega,t) = \sum_{j=0}^{N_{\rm p}(t)} \mathrm{e}^{-ij\omega T_{\rm p}} = \frac{1-\mathrm{e}^{-iN_p(t)\omega T_p}}{1-\mathrm{e}^{-i\omega T_{\rm p}}}, \tag{31}$$

quantity $\tilde{\aleph}^{(k)}$ can be represented as an inverse Fourier transform

$$\tilde{\aleph}^{(k)}(x,t) = F^{-1}[\mathfrak{I}^{(k)}(\omega,x,t)] \tag{32}$$

of the quantity

$$\mathfrak{I}^{(k)}(\omega,x,t) = \mathfrak{Z}(\omega,t)\mathcal{F}_k(\omega)\overline{Q}_{\rm las}(\omega,x,t)\mathrm{e}^{-i\omega\tau_k}. \tag{33}$$

Here $\tau_k = \langle \tau_r^{(jk)} \rangle_t$, where the mean value is taken over some observation time interval t, which is much larger than time between laser pulses.

Respective laser intensities can be introduced as

$$I_{\rm p}^{(k)} = \frac{c\epsilon_0 n}{2}[E_0^{(k)}]^2 = I_0 g^{(k)}, \tag{34}$$

where $g^{(k)}$ is the respective transition line gain–loss ratio. As well known, gain–loss ratios can be adjusted to almost the same level by the introduction of specific losses. For instance, these losses can be induced artificially either by injection of absorber in the laser cavity or by applying a liquid-crystal spatial light modulator. Then equal build-up times yield almost instantaneous oscillation kick off for each line, and laser intensities for each line can be adjusted to the same reference laser intensity, $I_{\rm p}^{(k)} = I_{\rm p}^{\rm ref}$.

Generalized result for spatial distribution of laser electric field amplification factor $Q_{\rm las}$, caused by multiple laser beam reflections inside the multi-pass cavity in the case of crosswise intersection with gas flow, obtained in Ref. [20], to the finite interval is given by

$$Q_{\rm las}(\omega,x,t) = \frac{iT(1-(\tilde{\rho}\tilde{\rho}_W)^{\frac{t}{\Delta t}})}{(1-\tilde{\rho}\tilde{\rho}_W)}\left[\tilde{\rho}\mathrm{e}^{i\alpha^{(1)}}\mathcal{D} + \mathrm{e}^{i\alpha^{(0)}}\right], \tag{35}$$

where $\Delta t = \frac{W_{\rm f}}{c}$, $T = 0.84$ and $\rho_W = 0.55$ are ZnSe window electric field transmission and reflectivity coefficients at a given wavelength:

$$\tilde{\rho}_W = \rho_W\mathcal{D}, \quad \tilde{\rho} = \rho\mathcal{D}, \quad \mathcal{D} = \exp\left(-\frac{\sigma_{\rm A}(\omega)n_i W_{\rm f}}{2}\right), \tag{36}$$

where $\rho = 0.9999$ is mirror strip electric field reflectivity, electric field phase is given by

$$\begin{cases} \alpha^{(0)} = \frac{\omega}{c}x + \frac{i\sigma_{\rm A}(\omega)n_i}{2}(x-\delta); \\ \alpha^{(1)} = \frac{\omega}{c}(2W_{\rm IC}-x) + \frac{i\sigma_{\rm A}(\omega)n_i}{2}(W_{\rm IC}-x-\delta), \end{cases} \tag{37}$$

where $W_{\rm IC} = 14.68$ cm is irradiation cell width.[7] As seen from Fig. 2, average amplification factor for intensity is almost the same for all, but near resonant frequencies, where significant dip is observed due to absorption by rarefied target gas.

6 Laser intensity variation range for the applicability of the SILARC method

As follows from Eqs. (27) and (32), excitation rate, corresponding to a pulsed multi-mode irradiation, can be estimated as $k_{\rm A} = \sum_{k=1}^{4} k_{\rm A}^{(k)}$, where excitation line of given isotopologue $k_{\rm A}^{(k)}$ is given by

$$k_{\rm A}^{(k)} = \frac{1}{\pi R_L^2}\sum_{i=1}^{N_l}\sum_{j=1}^{N_l} F^{-1}\left[\frac{\mathrm{d}\mathfrak{Z}^{(ijk)}}{\mathrm{d}\omega}\right], \tag{38}$$

[7] This value was taken from the previous results, published in Ref. [20].

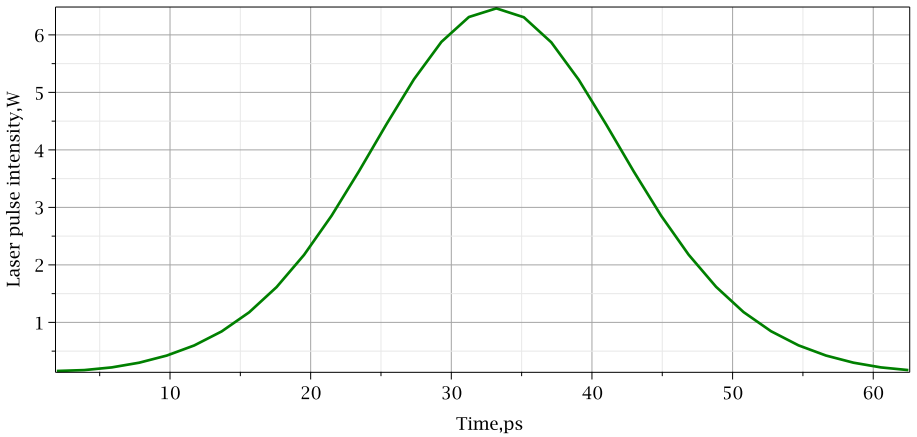

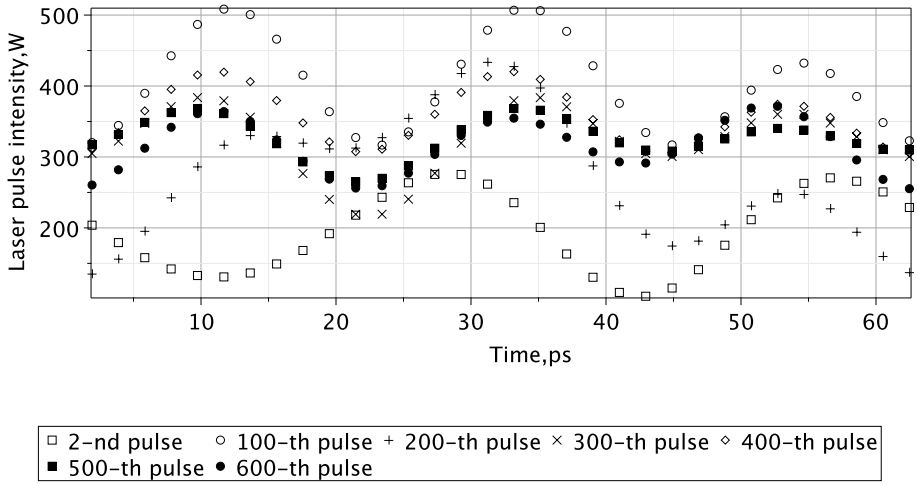

Fig. 3 Time evolution of laser field inside the resonant cavity over the time interval, corresponding to the N_pth laser shot: **a** $N_p = 1$; **b** $N_p = 100, 200, 300, 400, 600$. Energy per laser pulse is 20 nJ. One-line excitation by laser pulse with one-line laser spectrum is assumed: $\Delta\nu_p = 32\,\text{GHz}$; $\tilde{\lambda}_{1,\max}$. The number of Fourier transform nodes is $N_f = 2^5$, which corresponds to $t_{\max} = 116.4\,\text{ps}$ and $\nu_{\max} = 256\,\text{GHz}$

where

$$\frac{d\lambda^{(ijk)}}{d\omega} = \frac{1}{\hbar\omega}\frac{dW_A^{(ijk)}}{d\omega} \tag{39}$$

is the spectral number density of absorbed photons, and spectral energy density relation can be represented as

$$\frac{dW_A^{(ijk)}}{d\omega} = \sigma_k(\omega)\frac{c\epsilon_0 n}{2}E_0^{(i)}E_0^{(j)}\langle\aleph^{(i)}(x,t)\beth^{(j)}(\omega,x,t)\rangle_x. \tag{40}$$

In particular case of CW mode excitation, $\mathcal{F}(\omega) = \delta(\omega - \omega_{las})$, where ω_{las} is laser frequency, we obtain the following expression for excitation rate:

$$k_A = \frac{1}{\pi R_L^2}\frac{1}{\hbar\omega_{las}}\sigma_A(\omega_{las})I_{CW}. \tag{41}$$

To evaluate the inverse Fourier transforms, we use MapleSoft implementation of the fast Fourier transform (FFT) algorithm [33]. The maximal allowed interval in the frequency domain for a given time step t_{min} is restricted by the Nyquist frequency: $\nu_{\max} = 1/2t_{min}$, while the overall number of Fourier-transform nodes N_f in the frequency–time domain should be consistent with the condition for minimal frequency step ν_{min}:

$$\nu_{min}t_{min} = \frac{1}{N_f}. \tag{42}$$

To take advantage of FFT algorithm, we took the number of nodes N_f to fulfill condition $N_f = 2^{n_f}$. Since

$$t_{min} = \frac{t_{\max}}{N_f} \quad \nu_{min} = \frac{2\nu_{\max}}{N_f}, \tag{43}$$

the number of Fourier transform nodes is related to maximal frequency interval as

$$N_f = \nu_{\max}t_{\max}. \tag{44}$$

Results of our calculations for the laser pulse shape are shown in Figs. 3, 4, and 5 .

Average numbers of photons, resonantly absorbed by each isotopologue of BCl_3 molecule is given by

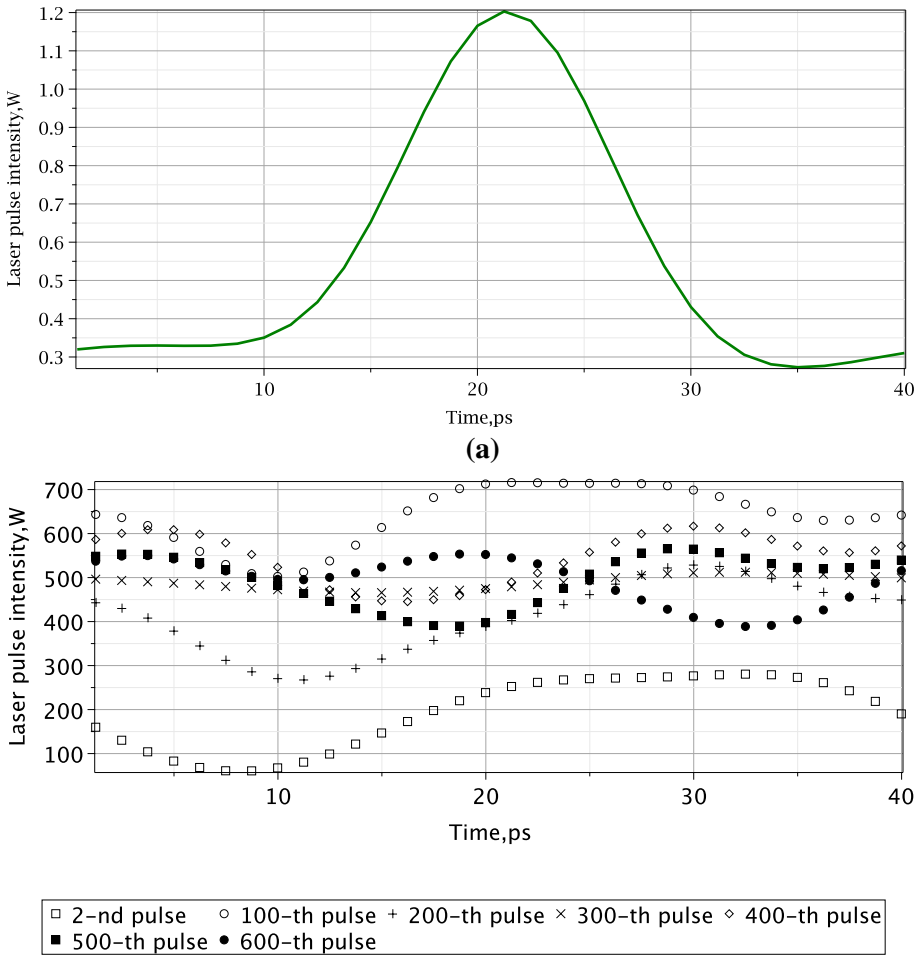

Fig. 4 Time evolution of laser field inside the resonant cavity over the time interval, corresponding to the N_pth laser shot: **a** $N_p = 1$; **b** $N_p = 100, 200, 300, 400, 600$. Energy per laser pulse is 20 nJ. One-line excitation by laser pulse with one-line laser spectrum is assumed: $\Delta\nu_p = 50\,\text{GHz}$; $\tilde{\lambda}_{1,\max}$. The number of Fourier transform nodes is $N_f = 2^5$, which corresponds to $t_{\max} = 74.5\,\text{ps}$ and $\nu_{\max} = 400\,\text{GHz}$

$$N_A^{(i)} = \int_0^{\tau_{ex}} dt k_A^{(i)}(t), \quad i = 1, \ldots, 4, \tag{45}$$

where excitation loss time coincides with the transition time of the gas flow across the laser beam $\tau_{ex} = \tau_{int}$, because all other relaxation times, caused by dimer formation, vibration–vibrational or vibration–translational transfers as well as spontaneous emission, are bigger [20].

To prevent multi-photon dissociation, the number of photons absorbed within excitation loss characteristic time interval should be less than $N_{crit} = \frac{D}{\epsilon_{crit}}$, where D is dissociation threshold, and $\epsilon_{crit} = h\nu_m$ is respective photon energy. Thus, according to Eq. (45), the upper limit for the laser intensity for given photo-absorption line is given by

$$I_{max}^{(k)} = I_{ref} \frac{\sigma_A(\nu_{k;las})}{h\nu_{k;las}} \frac{\phi_{crit}}{N_A^{(k)}}, \tag{46}$$

where it was taken into account that multi-photon absorption cross section is related to critical laser fluence $\phi_{crit} = 20\,\text{J}/cm^2$, Ref. [34], as $\sigma_{mp} = \frac{D}{\phi_{crit}}$.

The lower limit for applicability of the SILARC method, apparently, can be derived from the following condition:

$$I_{min}^{(k)} = \frac{I_{ref}}{N_A^{(k)}}. \tag{47}$$

Calculations below were carried out by assuming that multi-line laser pulse intensity I_p corresponds to CW-mode intensity $I_{ref} = I_{CW} = 1000$ W. In the case of choosing BCl_3 absorption spectrum, corresponding to $\tilde{\lambda}_1 = \tilde{\lambda}_{1,\max}$ and one-line excitation, the average numbers of photons, absorbed by each absorption line from 10P(8) emission line, are

$$\{N_A^{(1)}, N_A^{(2)}, N_A^{(3)}, N_A^{(4)}\} = \{10^{-3}, 0.008, 6.4, 1.56\}. \tag{48}$$

Thus, the lower and upper limits for the laser intensity in this case should be $I_{min}^{(3)} = 156.54\text{W}$ and $I_{max}^{(3)} = 693.4\,\text{MW}$.

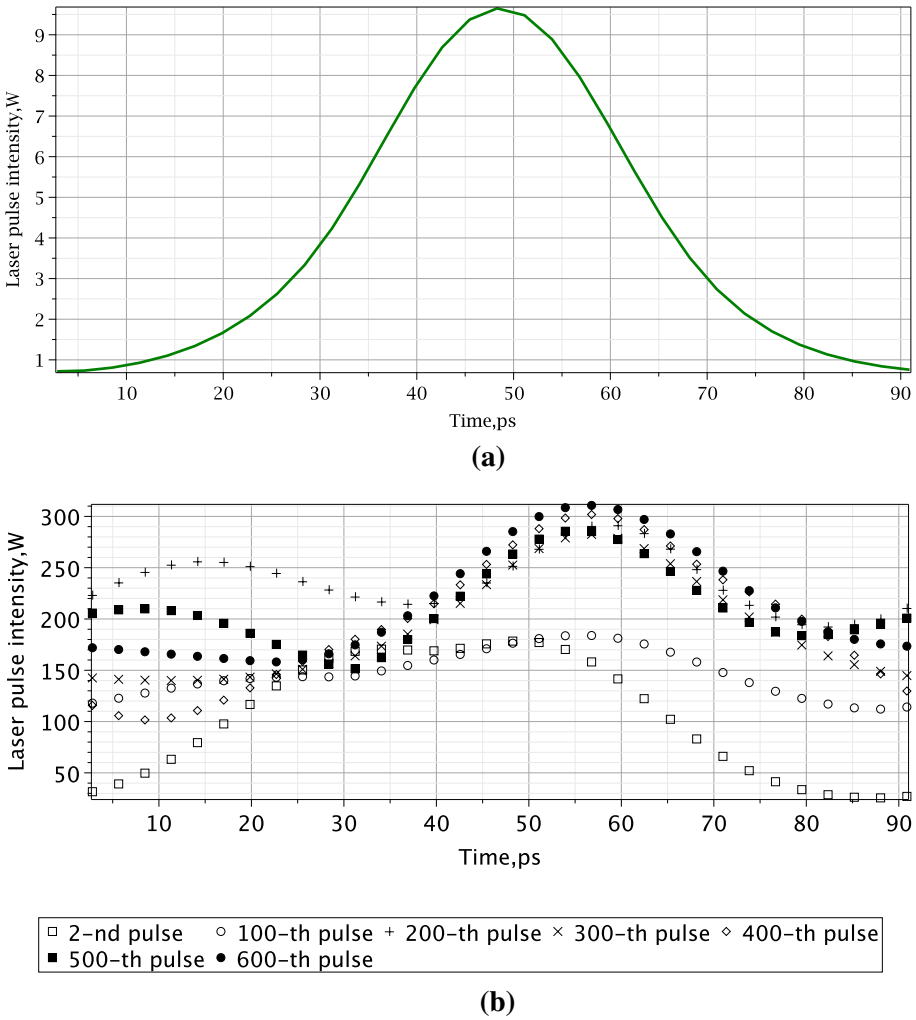

Fig. 5 Time evolution of laser field inside the resonant cavity over the time interval, corresponding to N_pth laser shot: **a** $N_p = 1$; **b** $N_p = 100, 200, 300, 400, 600$. Energy per laser pulse is 20 nJ. Four-line excitation by laser pulse with three-line laser spectrum is assumed: $\Delta\nu_p = 22\,\text{GHz}$; $\tilde{\lambda}_{1,\min}$. The number of Fourier-transform nodes is $N_f = 2^5$, which corresponds to $t_{\max} = 169.3\,\text{ps}$ and $\nu_{\max} = 176\,\text{GHz}$

In the case of two-line excitation, the average numbers of photons, absorbed by each absorption line from 10P(8) emission line, are

$$\{N_A^{(1)}, N_A^{(2)}, N_A^{(3)}, N_A^{(4)}\} = \{7.7 \times 10^{-3},\ 0.65,\ 2.22,\ 1.02\}. \tag{49}$$

Thus, the lower and upper limits for the laser intensity in this case should be $I_{\min}^{(3)} = 449.12\text{W}$ and $I_{\max}^{(3)} = 1.99\,\text{GW}$.

In the case of choosing BCl_3 absorption spectrum, corresponding to three-line excitation: $\tilde{\lambda}_1 = \tilde{\lambda}_{1,\min}$, calculated numbers of absorbed photons are

$$\{N_A^{(1)}, N_A^{(2)}, N_A^{(3)}, N_A^{(4)}\} = \{30.3,\ 2.2,\ 0.8,\ 0.02\}. \tag{50}$$

Thus, the lower and upper limits for the laser intensities should be as follows (Table 3).

Therefore, laser photons use efficiencies for $i = 1$, $i = 2$, and $i = 3$ photo-absorption lines excitation are following: $\eta_{\text{eff}}^{(1)} = 17.62\%$, $\eta_{\text{eff}}^{(2)} = 8.63\%$, $\eta_{\text{eff}}^{(3)} = 73.8\%$.

7 Summary

A new CO_2 laser system for multi-line boron isotopes separation is proposed. Its important characteristics such as an acceptable variation range of the laser power and pulse spectrum are computed. To do it, photo-absorption cross section for each chlorine isotopes combination in $^{11}B^{35}Cl_n^{37}Cl_{3-n}$ for $n = 1, 2, 3$ is recovered from the experimental data on infrared intensities, measured in gaseous state, and new formulas for the multi-mode laser pulse intensity and excitation rate are derived. Laser intensity acceptable variation ranges, which correspond to the applicability of the SILARC method, have been estimated from the average number of

Table 3 Constraints on the three-line laser pulse intensity

	$I_{\min}$, W	$I_{\max}$, GW
10P(8)	33	1.41
10P(10)	457.7	6.37
10P(12)	1197.5	5.34

photons absorbed by each chlorine isotopologue. These computations were carried out by taking into account multiple laser beam reflections in the resonant cavity and variation of photo-absorption spectrum center-line positions due to the ambiguity of available experimental data for BCl_3 in gaseous phase. Efficiencies of laser energy absorption for excitation by one, two, or three photo-absorption lines simultaneously in one laser pulse have been compared.

Acknowledgements Section 2 was supported by Project no. 1.669.2016/1.4 of the Russian Ministry of Science and Higher Education. Work on Sects. 3–6 was carried out at Steklov Mathematical Institute of Russian Academy of Sciences and supported by the Russian Science Foundation Grant 17-11-01388-P.

References

1. P.A. Bokhan, V.V. Buchanov, N.V. Fateev, M.M. Kalugin, M.A. Kazaryan, A.M. Prokhorov, D.E. Zakrevsky, *Laser Isotope Separation in Atomic Vapor* (WILEY-VCH Verlag GmbH & Co. KGaA, Weinheim, 2006)
2. Jifa Tian, Jinming Caia, Chao Hui, Chengdong Zhang, Lihong Bao, Min Gao, Chengmin Shen, Hongjun Gaoa, Boron nanowires for flexible electronics. Appl. Phys. Lett. **93**, 122105-1–122105-3 (2008)
3. Zhuhua Zhang, Andrew J. Mannix, Hu Zhili, Brian Kiraly, Nathan P. Guisinger, Mark C. Hersam, Boris I. Yakobson, Substrate-induced nanoscale undulations of borophene on silver. Nano Lett. **16**(10), 6622–6627 (2016)
4. P. Singh, S.N. Singh, M. Lal, M. Husain, Temperature dependence of I–V characteristics and performance parameters of silicon solar cell. Sol. Energy Mater. Sol. Cells **92**, 1611–1616 (2008)
5. P. Singh, N.M. Ravindra, Temperature dependence of solar cell performance-an analysis. Sol. Energy Mater. Sol. Cells **101**, 36–45 (2012)
6. D.M. Adams, W. Ji, R.F. Barth, Comparative in vitro evaluation of dequalinium B, a new boron carrier for neutron capture therapy (nct). Anticancer Res. **20**(5B), 3395–3402 (2000)
7. W.S. Kiger et al., A pharmacokinetic model for the concentration of B-10 in blood after boronophenylalanine–fructose administration in humans. Radiat. Res. **155**(4), 611–618 (2001)
8. R.F. Barth, Boron neutron capture therapy at the crossroads: challenges and opportunities. Appl. Radiat. Isot. **67**, S3–S6 (2009)
9. D.J. Tannor, *Introduction to Quantum Mechanics: A Time Dependent Perspective* (University Science Press, Sausalito, 2007)
10. V.S. Letokhov, *Laser Control of Atoms and Molecules* (Oxford University Press, Oxford, 2007)
11. Y.T. Lee, Isotope separation by photodissociation of Van der Waal's molecules. US Patent 403,230,6, 28 June (1977)
12. J.W. Eerkens, Laser-induced migration and isotope separation of epi-thermal monomers and dimers in supercooled free jets. Laser Part. Beams **23**, 225–253 (2005). https://doi.org/10.1017/S0263034605225325X
13. E.R. Grant, P.A. Schulz, A.S. Sudbo, Y.R. Shen, Y.T. Lee, Is multiphoton dissociation of molecules a statistical thermal process? Phys. Rev. Lett. **40**, 115–118 (1978)
14. P. Lavigne, J.L. Lachambre, Pressure dependent absorption in BCl_3 at 10.6 μm. Appl. Phys. Lett. **19**, 176–179 (1971)
15. N.V. Karlov, Y.N. Petrov, A.M. Prokhorov, O.M. Stel'mach, Dissociation of boron trichloride molecles by CO_2 laser radiation. ZhETF Pis. Red. **11**(4), 220–222 (1970)
16. R.V. Ambartzumian, V.S. Letokhov, E.A. Ryabov, N.V. Chekalin, Isotopic selective chemical reaction of BCl_3 molecules in a strong infrared laser field. J. Exp. Theor. Phys. Lett. **20**, 273–274 (1974)
17. J.L. Lyman, S.D. Rockwood, Enrichment of boron, carbon, and silicon isotopes by multiple photon absorption of 10.6μm laser radiation. J. Appl. Phys. **47**, 595 (1976). https://doi.org/10.1063/1.322619
18. A.K. Nayak, S.K. Sarkar, Modelling of multifrequency IRMPD for laser isotope separation. Proc. Indian Acad. Sci. (Chem.) **114**(6), 649–657 (2002)
19. M. Kumar, V. Gupta, A.K. Nath, Efficient laser isotope separtion of ^{13}C using novel linear multi-pass cavity. Appl. Phys. B **80**, 757–763 (2005)
20. K.A. Lyakhov, H.J. Lee, A.N. Pechen, Some features of boron isotopes separation by the laser-assisted retardation of condensation method in multipass irradiation cell implemented as a resonator. IEEE J. Quantum Electron. **52**, 1400208-1–8 (2016)
21. W.J. Witteman, *The CO2 Lasers, Ch. Short-Pulse Amplification* (Springer, Berlin, 1987), pp. 23–52
22. Jens Spanget-Larsen, Infrared Intensity and Lorentz Epsilon Curve from 'Gaussian' FREQ Output. https://www.academia.edu/24081699/Infrared_Intensity_and_Lorentz_Epsilon_Curve_from_Gaussian_FREQ_Output. Accessed 29 June 2015
23. D.F. Wolfe, G.I. Humphrey, Force constants for pure and mixed halides of boron. J. Mol. Struct. **3**, 293–303 (1969)
24. W.B. Maier II, R.F. Holland, High resolution infrared absorption spectra of BCl_3 and BCl_2F dissolved in solid argon and krypron. J. Chem. Phys, **72**(12), 6661–6677 (1980)
25. PaR Systems, (2018). https://www.par.com/technologies/pulsed-co2-lasers/high-pressure-te-co2-lasers/
26. H. Houfman, J. Meyer, Ultrashort CO_2 laser pulse generation by square-wave mode locking and cavity dumping. Opt. Lett. **12**, 87–89 (1987)
27. M.N. Polyanskiy, I.V. Pogorelsky, V. Yakimenko, Picosecond pulse amplification in isotopic CO_2 active medium. Opt. Express **19**(8), 7117–7125 (2011)
28. H. Bergmann, High pressure CO_2 amplifiers for picosecond pulse amplification. In: Proceedings SPIE 11042, XXII International Symposium on High Power Laser Systems and Applications (2019). https://doi.org/10.1117/12.2522314
29. O.R. Wood, R.L. Abrams, T.J. Bridges, Mode locking of a transversely excited atmospheric pressure CO_2 laser. Appl. Phys. Lett. **17**, 376–378 (1970)
30. A.E. Siegman, D.J. Kuizenga, Simple analytical expressions for AM and FM mode-locked pulses in homogeneous lasers. Appl. Phys. Lett. **14**, 518–520 (1969)
31. D.J. Kuizenga, A.E. Siegman, FM and AM mode locking of the homogeneous laser. IEEE J. Quantum Electron. **QE–6**(11), 694–708 (1970)
32. R.L. Abrams, O.R. Wood, Characteristics of a mode-locked TEA CO_2 laser. Appl. Phys. Lett. **19**, 518–522 (1971)
33. Maplesoft, (2018). http://www.maplesoft.com. Accessed 27 Sept 2017
34. V.S. Bagratashvili, V.N. Letokhov, A.A. Makarov, E.A. Ryabov, *Multiple Photon Infrared Laser Photophysics and Photochemistry* (OPA, Amsterdam, 1985)